Heterogeneous Uptake Kinetics of Volatile Organic Compounds on Oxide Surfaces Using a Knudsen Cell Reactor: Adsorption of Acetic Acid, Formaldehyde, and Methanol on α-Fe_2O_3, α-Al_2O_3, and SiO_2

S. Carlos-Cuellar,[†] P. Li,[†,§] A. P. Christensen,[†,§] B. J. Krueger,[†] C. Burrichter,[§] and V. H. Grassian*[,†,‡,§]

Department of Chemistry, Department of Chemical and Biochemical Engineering, and the Center for Global and Environmental Research, University of Iowa, Iowa City, Iowa 52242

Received: August 14, 2002; In Final Form: January 30, 2003

The role of heterogeneous reactions on particulate matter present in the Earth's atmosphere remains an important question in tropospheric chemistry. It has been proposed in several modeling studies that mineral dust may provide reactive surfaces for trace atmospheric gases. Laboratory studies can provide some answers concerning the kinetics of these reactions, so that heterogeneous chemistry can be quantitatively assessed in atmospheric chemistry models. In this study, the heterogeneous uptake kinetics of several volatile organic compounds (VOCs) on oxide surfaces have been measured with a Knudsen cell reactor at 295 K. In particular, the heterogeneous uptake of acetic acid, methanol, and formaldehyde on α-Fe_2O_3, α-Al_2O_2, and SiO_2 has been investigated. These VOCs are representative of some of the different types of oxygenated organics found in the atmosphere. The oxide particles used in this study are models for mineral dust found in the Earth's atmosphere. Initial uptake coefficients, γ_0, have been extracted from the Knudsen cell data. The uptake kinetics have been measured as a function of sample surface area to ensure that realistic surface areas are used in the calculation of the uptake coefficient. Heterogeneous reaction rates are then compared to homogeneous reactions rates for gas-phase reactions involving acetic acid, methanol, and formaldehyde. From this comparison, the possible atmospheric implications of heterogeneous reactions involving these oxygenated organics are discussed.

Introduction

The heterogeneous chemistry of volatile organic compounds (VOCs) on aerosol surfaces and its overall significance in the atmosphere are not well-known. Therefore, laboratory studies are needed to quantify what reactions take place on aerosol surfaces and how they impact the chemistry of the atmosphere. VOCs present in the earth's atmosphere play a major role in air pollution. Heterogeneous reactions that can alter VOC concentrations have important implications for tropospheric ozone formation. Ozone is not directly emitted into the troposphere but is formed through a complex series of photochemical reactions involving nonlinear interactions among NO_x, volatile organic compounds (VOCs), and carbon monoxide.[1] A recent study showed that tropospheric ozone production efficiencies from NO_x emissions were controlled by the abundance of VOCs.[2] Thus, sources and sinks of VOCs must be well understood.

VOCs are directly emitted into the atmosphere from both natural and anthropogenic sources.[3] Organics can readily undergo chemical transformations in the atmosphere and are oxidized with a variety of oxidizing agents such as atomic oxygen, hydroxyl radical, peroxy radical, molecular oxygen, ozone, and hydrogen peroxide as well as with ClO_x, BrO_x, and NO_x. Oxidation reactions lead to the formation of a variety of oxygenated organics including organic acids, alcohols, and carbonyl compounds, to name a few.[3−6] These compounds are of interest in atmospheric chemistry because many of them have been linked to upper tropospheric NO_x and HO_x cycles.[7]

Although there is some question as to all of the sources of organic acids, such as acetic acid in the atmosphere, it is known that both primary and secondary sources of acetic acid exist.[8] Acetic acid is one of the most abundant carboxylic acids in the troposphere. Concentrations of acetic acid reported in the literature vary by location, season, and time of day (from 0.05 to 16 ppbv gas-phase acetic acid).[9] They are usually higher during the day, during the dry season, and in urban areas. Primary sources include anthropogenic emissions from biomass combustion and vehicular emissions, and biogenic emissions from soil and vegetation.[9] Secondary sources consist of the photochemical oxidation of chemical precursors, as for example, the reaction of isoprenes and monoterpenes with ozone.[9] Removal processes for acetic acid in the troposphere are comprised principally of wet and dry deposition, and to a smaller extent direct photolysis and reaction with OH radicals in the upper troposphere.[9] Single-particle and spectrochemical studies have shown that there are many tropospheric particles that contain organic acids.[10,11] How these organic acids interact with tropospheric particles is, therefore, of interest.

It has long been known that formaldehyde and other carbonyls such as acetone play an important role in the photochemical oxidant cycle, being produced by the photooxidation of most VOCs and, in-turn, serving as an important source of peroxy radicals and peroxyacyl nitrates.[3] Their dual role makes them an important species for testing the performance of photochemical oxidant models. However, little is known about carbonyls in the troposphere, since only a few are routinely measured in monitoring programs and measurement campaigns (most com-

* To whom correspondence should be addressed.
[†] Department of Chemistry.
[‡] Department of Chemical and Biochemical Engineering.
[§] Center for Global and Environmental Research.

10.1021/jp0267609 CCC: $25.00
Published on Web 05/07/2003

monly measured are formaldehyde, acetaldehyde, and acetone). Formaldehyde is one of the most prevalent carbonyl compounds in the Earth's atmosphere. Methanol is another volatile organic compound of great interest because it is a globally abundant organic species with poorly understood sources and removal processes.[7] The 1997 Subsonic Assessment (SASS) Ozone and Nitrogen Oxide Experiment (SONEX) discovered large differences between atmospheric concentrations and estimated sources of methanol.

The transport of organic pollutants in the atmosphere is strongly affected by their tendency to adsorb to aerosol particles or to terrestrial surfaces. It is thought that the adsorption to the surface of mineral oxides or salts is one of the relevant processes.[12] Additional knowledge of heterogeneous processes, such as reactions on the surface of mineral dust aerosol, could identify effective sinks and provide a greater understanding of the earth-atmosphere system. In general, oxygenated organics with functional groups such as carboxylic acids will have a greater tendency to adsorb to surfaces.

In this study the heterogeneous uptake of acetic acid, formaldehyde, and methanol is investigated. These compounds are used as a subset of representative oxygenated organics found in the Earth's atmosphere. In particular, the heterogeneous uptake of acetic acid, methanol, and formaldehyde on the oxides of some of the most abundant elements present in the Earth's crust, including SiO_2, α-Fe_2O_3, and α-Al_2O_3, has been measured. These oxides were used as models for mineral dust found in the atmosphere. A Knudsen cell reactor was used to measure heterogeneous reaction kinetics at 295 K. The data have been analyzed in terms of a heterogeneous uptake coefficient, γ. The data generated in this study can be used as input in global atmospheric models as an additional sink for these compounds. As will be discussed, the importance of these heterogeneous reaction pathways will depend on whether these reactions are fast enough to compete with gas-phase chemical and photochemical reactions. Only in cases of comparative rates will heterogeneous reaction have an appreciable effect on the chemical balance of the troposphere. In addition, infrared spectroscopy was used to glean information about the nature of the organic−oxide interaction.

Experimental and Data Analysis Section

Knudsen Cell Reactors—Principles of Operation. Knudsen cell reactors are very low-pressure flow reactors that can be used to obtain kinetic information for heterogeneous gas−solid and gas−liquid reactions.[13] The technique is ideally suited for the study of heterogeneous reactions in that, at the experimental pressures used, the mean free path of the molecules in the cell usually exceeds the dimensions of the cell. This minimizes the possibility of gas-phase collisions and eliminates boundary layer effects, which greatly simplifies the analysis of the data.

The general design of Knudsen cell reactors for the study of heterogeneous reactions has been described in detail in the literature.[13−15] Typically, the reactor consists of a chamber with an isolated sample compartment and a small aperture through which gas-phase reactant and product species can escape to be detected, usually by mass spectrometry. The choice of the size of the aperture (or hole), A_h, and the volume of the reactor, V, determines the escape constant, k_{esc}, that is, the first-order rate constant, of the molecules through the cell, as shown in eq 1,

$$k_{esc} = \frac{\bar{c}A_h}{4V} \qquad (1)$$

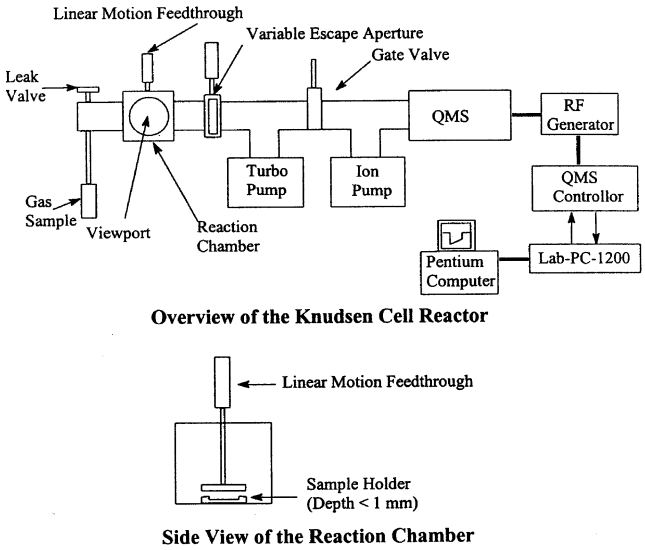

Figure 1. Single-stage Knudsen cell reactor used to measure heterogeneous reaction kinetics.

where $\bar{c}$ is the average molecular speed of the gas molecules. Although k_{esc} can, in principle, be calculated using eq 1, it is more typical to experimentally determine k_{esc}, because of limited conductance of the vacuum system (vide infra).

Two different types of Knudsen cell reactors were used in these experiments: a single-stage sample holder Knudsen cell reactor and a multistage sample holder reactor. There are advantages and disadvantages to using each of these. The obvious advantage of the multistage Knudsen cell reactor is that different samples (either different powders or the same powder but different masses) can be analyzed in a single experiment. The disadvantage is that the volume of the reactor tends to be large (on the order of 1000 cm^3) and, thus, limits the values of k_{esc} that can be reasonably obtained. The advantage of the single-stage Knudsen cell reactor is that the volume of the reactor can be made much smaller (on the order of 100 cm^3), and thus, k_{esc} values as large as 5−10 s^{-1} can be obtained. The single-stage Knudsen cell reactor was used to measure the heterogeneous reaction kinetics of acetic acid and formaldehyde on oxide particles.[16] The single-stage Knudsen cell reactor is shown in Figure 1. The reactor consists of a stainless steel cross that serves as the reaction chamber. The reaction chamber is coupled to an UTI-100C quadrupole mass spectrometer (QMS) through a gate valve. The mass spectrometer is pumped by a 150 L/s ion pump (Varian). The region between the exit aperture and the gate valve can be differentially pumped by a 70 L/s turbomolecular pump (Varian). Gas molecules are introduced into the reaction chamber through a leak valve. A stainless steel sample holder sits on top of a tee support in the reaction chamber and is O-ring sealed by a blank flange. Two different sample holders were used in these experiments with geometric areas, A_s, of 11.96 and 5.34 cm^2. The blank flange is attached to a push−pull linear motion feedthrough, so the sample holder can be completely and quickly opened by pulling up on the linear motion feedthrough. The volume of the sealed sample holder is small, such that when the sample holder lid is lifted and opened, there is no observed drop in gas pressure if no powder is present. A variable iris is used to adjust the size of the escape aperture.

The multistage Knudsen cell reactor was used in several experiments to measure the heterogeneous kinetics of methanol uptake on oxide particles. A schematic of the reaction chamber of the multisample Knudsen cell is shown in Figure 2. It consists of a stainless steel reducing cross (6−2.75 in.) with four

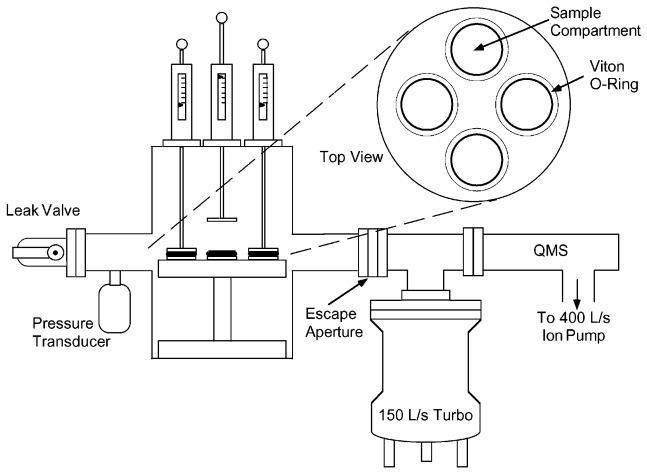

Figure 2. Multistage Knudsen cell reactor used to measure heterogeneous reaction kinetics.

individual sample holders attached to a platform that rests on the bottom of a 6 in. flange. All exposed interior surfaces are coated with Teflon. Four Teflon coated aluminum disks attached to four linear translators serve as covers for each of the powdered samples. The geometric area of each of the four sample holders is 5.07 cm^2. Since the volume of the sample holder is much smaller than the total volume of the reactor (~1500 cm^3), no corrections are needed to account for volume change upon opening the sample compartment. The seal between the sample holders and the cover is made with viton O-rings. With this setup, four different samples are analyzed in a single run.

The multistage Knudsen cell reactor is also coupled to a QMS (UTI, DetecTorr II). The mass spectrometer is housed in a vacuum chamber equipped with a 400 L/s ion pump and an ion gauge (both from Varian). The region between the quadrupole mass spectrometer and the Knudsen cell reactor is pumped by a 150 L/s turbomolecular pump (Leybold) for differential pumping of the mass spectrometer.

The experimentally determined first-order escape constants used in these experiments were determined by abruptly changing the inlet flow of each gas while monitoring the QMS signal intensity of the parent ion as a function of time. A plot of the natural log of the QMS signal intensity as a function of time gave a straight line of slope equal to $-k_{esc}$. For the three gases investigated, the following ions were monitored with the QMS; $m/e = 60$ (CH_3COOH^+) for CH_3COOH, $m/e = 29$ (CHO^+) for CH_2O, and $m/e = 31$ (CH_3O^+) for CH_3OH.

Samples for the Knudsen cell experiments were prepared by either using an atomizer to spray an aqueous slurry of the sample onto a slightly heated sample holder or by allowing a hydrosol of the oxide particles to dry in the sample holder. Both of these procedures ensured even coverages of the powdered sample across the bottom of the sample holder, as determined with an optical microscope. The samples were put in the Knudsen reactor and evacuated overnight. Evacuation times were kept constant in order to obtain reproducible data. This observation suggests that water on the surface of the oxide particles can play a role in the uptake of the gases under investigation as the amount of surface hydration changes with evacuation time. Although most of the surface adsorbed water is removed upon evacuation, the surface of theses oxide particles is covered with hydroxyl groups and there is a residual amount of more strongly bound water that is not removed by evacuation at 295 K.[17]

For all Knudsen cell experiments, flowing the reactive gas through the reactor for at least 90 min prior to the experiment passivated the walls of the reactor. The gas was introduced through a leak valve to the desired pressure, as measured with an absolute pressure transducer (MKS 690A.1TRC range 10^{-6} to 0.1 Torr). During passivation the powdered samples were sealed with the blank flange. The Knudsen cell sample holders have been designed such that there is minimal volume change when the sample lid is opened.

Several blank experiments were done in these studies. One set of experiments was done with no sample powder in place to determine if any uptake occurred on the surface of the sample holder. No uptake was observed on the sample holder lid for any of the VOCs investigated. In another set of experiments, the uptake of several nonreactive gases such as N_2, Ar, and He was investigated on the oxide powders. In all of these experiments, there was no change in signal observed when the sample holder was open to N_2, Ar, or He, indicating that these gases were not taken up on the oxide surfaces at 295 K.

Knudsen Cell Reactors—Data Analysis. From the Knudsen cell data, it is useful to determine a heterogeneous uptake coefficient, γ, which is simply a measure of how likely the molecule will be taken up by the surface, through either adsorption or reaction, per a gas-phase collision basis. It is defined by eq 2:[18]

$$\gamma = (\text{the net loss of molecules from the gas phase to the surface per second})/(\text{the total number of gas–surface collisions per second}) \quad (2)$$

By considering gas flow through the Knudsen cell reactor in the presence and absence of a reactive surface, a steady-state uptake coefficient can be derived.[13−15] In the presence of a reactive surface, there is a competition between gas flow out of the escape aperture or hole, A_h, and molecules being taken up by the surface.

The steady-state uptake coefficient for a first-order reaction is given in eq 3:

$$\gamma = \frac{A_h}{A_s}\left(\frac{F_0 - F}{F}\right) = \gamma_{obs} \quad (3)$$

In deriving eq 3, it is typical to use the geometric area of the sample holder, A_s. The term F_0 represents the flow of gas in the absence of a reactive surface (i.e. when the sample lid is closed to the powdered sample), and F represents the flow of gas in the presence of a reactive surface. Both A_s and A_h are calculated from the measured diameters of the geometric sample holder and the aperture hole, respectively. The reported value of A_h is corrected for the Clausing factor and is thus an effective aperture.[19]

Since the measured quantity is usually the mass spectral intensity of the reactant gas and this value is directly proportional to the flow out of the cell, eq 3 usually appears as

$$\gamma = \frac{A_h}{A_s}\left(\frac{I_0 - I}{I}\right) = \gamma_{obs} \quad (4)$$

Here I_0 and I are the mass spectral intensities measured in the absence and presence of a reactive surface, respectively. For the reasons described below, the uptake coefficient calculated using eqs 3 and 4 will be referred to as the observed uptake coefficient, γ_{obs}.

There are several assumptions made in the derivation of eqs 3 and 4. The first assumption is that the geometric area of the sample holder, A_s, is appropriate in considering the total number of gas–surface collisions. However, for a powdered sample

there may be some diffusion into the powder on the time scale of the measurement (on the order of seconds), and therefore the surface area and thus the number of collisions will be greater than that calculated using A_s. Correcting the observed uptake coefficient for this increased surface area requires an understanding as to how gas molecules diffuse into the powder during the time scale of the measurement.

In 1991, Keyser, Moore, and Leu (KML) adapted a model from the heterogeneous catalysis literature[20] to explain heterogeneous reactions of atmospheric relevance.[21] The model takes into account gas diffusion into the underlying layers of a porous sample by considering the surface area contribution from both the first layer (external) and underlying layers (internal) of particles in determining uptake coefficients.[21,22] As the earlier work includes a complete set of justifications and derivations[20−22] that has been summarized in other publications,[19,23,24] the details will not be presented here. The premise of the model is that the true uptake coefficient, γ_t, can be thought of in terms of external and internal components which are related to the observed uptake coefficient, γ_{obs}, by the following equation,

$$\gamma_{obs} = \gamma_t \left(\frac{S_e + \eta S_i}{A_s} \right) \tag{5}$$

where

$$\eta = \frac{1}{\phi} \tanh(\phi)$$

and

$$\phi = \left(\frac{m}{\rho_b A_s d} \right) \left(\frac{3\rho_b}{2(\rho_t - \rho_b)} \right) (3\tau\gamma_t)^{1/2}$$

The parenthetic term following γ_t is a correction factor for the effect of gas-phase diffusion into the underlying layers. S_i and S_e are the internal and external surface areas, respectively, A_s is the geometric area of the sample holder, and η is a calculated "effectiveness factor". The effectiveness factor is the fraction of the internal area that contributes to the measured value of the uptake coefficient. Its value is mass (sample thickness) dependent and is determined from the relative rates of surface adsorption and diffusion into the underlying layers. Because of inhomogeneities in the interparticle voids, however, the effective diffusion constant is less than would be calculated assuming diffusion through long straight capillaries. This effect is accounted for by incorporating a tortuosity factor, τ. Porous solids have predicted τ values in the range 1−8. However, most porous solids, especially powders, are not characterized well enough for an accurate calculation of τ to be made; thus, τ must be experimentally determined. Other parameters in eq 5 include the mass of the sample, m, the true density of the material, ρ_t, the bulk density of the powder, ρ_b, and the diameter of the particles, d, as discussed in ref 19.

The form of the equation that we use in our studies is somewhat modified from the work by others in that here we do not assume either simple cubic or hexagonal close-packing spheres. Instead, the experimentally measured bulk density was used in the calculations.[19] In addition, the specific BET surface area was measured rather than calculated. Rewriting eq 5 in terms of measured bulk density and BET surface area yields

$$\gamma_{obs} = \gamma_t \rho_b S_{BET} (h_e + \eta h_i) \tag{6}$$

where S_{BET} is the BET specific surface area, h_e is the height of the first layer, and h_i is the height of all the internal layers calculated from the total mass, the measured bulk density, and the particle mass.

As will be shown here, there are two regimes evident in plots of observed uptake coefficient, γ_{obs}, versus mass. Since the sample holder geometric area remains constant, increasing the mass of the powdered sample increases the number of particle layers and thus the total height of the internal layer. The first regime is seen at low masses when there are a few layers of particles. In this regime, the observed initial uptake coefficient has a linear dependence on the sample mass and the number of particle layers. This linear dependence arises because for thin samples reactant gas molecules can diffuse through the entire sample on the time scale of the measurement. In this situation, the entire sample area contributes to the observed uptake coefficient and extracting the true uptake coefficient from the observed uptake coefficient requires consideration of both the entire reactive area and the resultant increase in the number of collisions a molecule makes within the depth of the powdered sample. As shown below, this leads to a very simple correction factor that will work for any adsorbate/powder system for which this linear mass regime can be measured. The second regime, which is termed the plateau regime, occurs at higher masses. In the plateau regime, the value of γ_{obs} is independent of sample mass. This independence of sample mass arises because in the plateau regime the gas molecules only diffuse through a portion of the powder on the time scale of the measurement. Typically, when no mass dependence is reported in these types of experiments it is because the experiments are being done in the plateau region. The extent of the linear regime depends on the value of the true uptake coefficient, the particle size and BET area, the powder density, and the tortuosity whereas the slope of the linear regime depends only on the true uptake coefficient and the size and surface area of the particles.

As mentioned above, there is a simple way to determine the true uptake coefficient using a simple correction factor that will work for any gas/powder system in which the linear mass regime can be measured. In the linear region the incoming molecules can access all of the particles and a correction for the "internal" collisions in the lower layers of the powdered sample must also be found.[19,24] The correction can be made by using the total BET area of the sample, and eq 4 becomes

$$\gamma_t = \frac{A_h}{A_{BET}} \left(\frac{I_0 - I}{I} \right) = \left(\frac{A_s}{A_{BET}} \right) \gamma_{obs} \tag{7}$$

For masses in the linear mass-dependent (LMD) regime, the observed uptake coefficient calculated via eq 4 can be measured and plotted as a function of sample mass. The best-fit slope of this line can be used to determine the true uptake coefficient as follows,[19,24]

$$\gamma_t = \text{slope } (\text{mg}^{-1}) \frac{A_s\ (\text{cm}^2)}{S_{BET}\ (\text{cm}^2\ \text{mg}^{-1})} \tag{8}$$

if the specific surface area defined here as the specific BET area, S_{BET}, for the oxides is known.

FT-IR Measurements. Oxide samples for FT-IR analysis were prepared by pressing powdered samples of the oxide onto a tungsten grid.[16,24] Approximately 25 mg of the powder was evenly coated onto a 3 cm × 1 cm area of the grid. Only half of the grid was pressed with the oxide powder, and the other half was left blank. Once the tungsten grid was coated with the oxide, the grid was mounted inside the IR cell. The IR cell used

in these experiments has been described previously.[24] Briefly, the IR cell consists of a stainless steel cube that is attached to a vacuum system consisting of an 80 L/s ion pump and a 60 L/s turbomolecular pump.

The IR cell was held in place by a linear translator inside the sample compartment of a Mattson RS-1 FT-IR spectrometer equipped with a narrow band MCT detector. The linear translator allows each half of the sample grid to be translated into the infrared beam. This permits the investigation of gas-phase and adsorbed species on the oxide surface under identical reaction conditions. Each spectrum was recorded by averaging 250 scans at an instrument resolution of 4 cm^{-1}. Each absorbance spectrum shown represents a single beam scan referenced to the appropriate single beam scan of the clean oxide sample or the blank grid prior to gas introduction, unless otherwise noted.

Sources of Oxide Powders and VOCs Used in This Study. The oxide particles used in these experiments were purchased from commercial sources. Several different oxides were used in these studies. Unless otherwise noted, α-Fe_2O_3 (Aldrich, 99+%), α-Al_2O_3 (Alfa Aesar, 99.99%), and SiO_2 (Degussa) powders with BET measured surface areas of 2.9, 12.8, and 225 m^2/g, respectively, were used. The particles in these samples have average particle diameters of 0.69 μm (α-Fe_2O_3), 1.0 μm (α-Al_2O_3), and 0.02 μm (SiO_2), as determined by scanning electron microscopy. The vapors from liquid methanol (Fisher Scientific, 99.9% purity) and anhydrous acetic acid (Alpha Aesar, 99.9985% purity) were used in these studies. The liquid samples were subjected to several freeze−pump−thaw cycles prior to use. Formaldehyde was prepared by heating and decomposing paraformaldehyde. Gas-phase formaldehyde was stored in a glass bulb. Formaldehyde samples were freshly prepared every day.

Results and Discussion

Heterogeneous Uptake of Acetic Acid, Formaldehyde, and Methanol on Oxide Surfaces: Knudsen Cell Measurements. The heterogeneous uptake of acetic acid, formaldehyde, and methanol was measured on three different oxides α-Fe_2O_3, α-Al_2O_3, and SiO_2. The Knudsen cell data, plotted as QMS intensity as a function of time, for acetic acid, formaldehyde, and methanol, are shown in Figures 3−5, respectively. As discussed in the Experimental Section, a steady-state flow is established in the reactor before the experiment begins. For acetic acid the pressure in the Knudsen cell reactor was kept at 6 μTorr, corresponding to a gas concentration of 1.9×10^{11} molecules cm^{-3}. The data shown in Figure 3 are for acetic acid uptake on 10.6 mg of α-Fe_2O_3, 64.0 mg of α-Al_2O_3, and 25.0 mg of SiO_2. (In the acetic acid experiments, SiO_2 purchased from Strem Chemicals with a surface area of 1.6 m^2/g was used.) It can be seen that there is a decrease in the QMS signal when the oxide sample is exposed to gas-phase acetic acid, as indicated by the rectangular bar marked"open"in the figure. During this time, the sample holder lid is in the open position and the acetic acid can adsorb onto the particle surface. The drop in the QMS signal is greatest at the beginning when the particles are first exposed to the acetic acid. When the sample lid is closed, the acetic acid signal goes back to its original baseline value.

Similar Knudsen cell data are seen for the other two VOCs investigated. Formaldehyde uptake on 19.6 mg of α-Fe_2O_3, 7.1 mg of α-Al_2O_3, and 2.3 mg of SiO_2 is shown in Figure 4, and methanol uptake on 18.8 mg of α-Fe_2O_3, 6.0 mg of α-Al_2O_3, and 6.2 mg of SiO_2 is shown in Figure 5. In the case of formaldehyde uptake on α-Fe_2O_3 and α-Al_2O_3, the sample

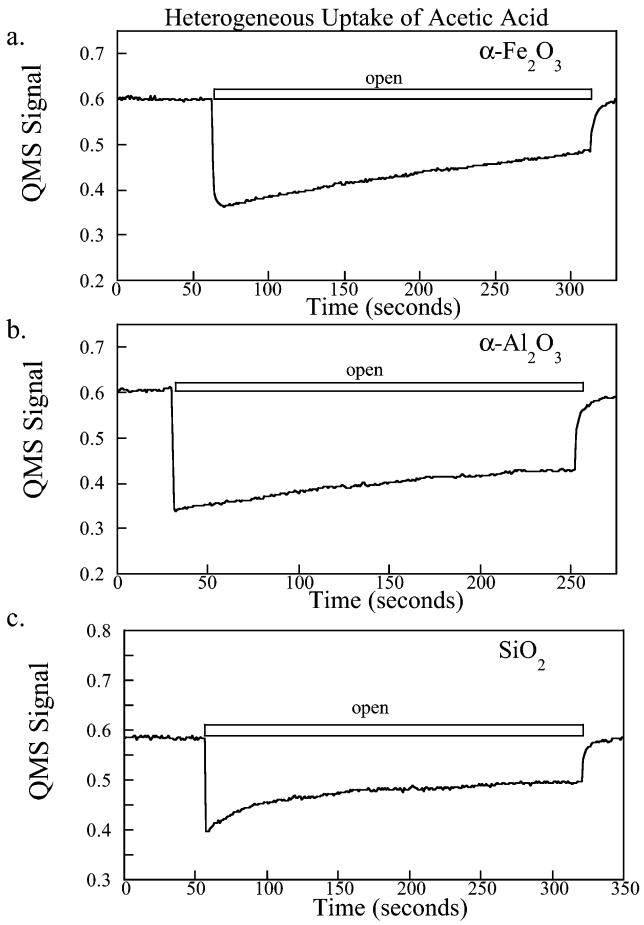

Figure 3. Knudsen cell data (QMS intensity versus time) for the heterogeneous uptake of acetic acid on 10.6 mg of α-Fe_2O_3, 64.0 mg of α-Al_2O_3, and 25.0 mg of SiO_2. The gas pressure inside the reactor was 6 μTorr measured, and the measured $k_{esc} = 2\ s^{-1}$.

holder lid was opened and closed twice for 100 s each time. These data show that, after first establishing a steady state flow and a stable QMS signal, the signal decreases the first time the sample lid is opened, exposing the particles to gas-phase formaldehyde, and then returns to its initial value when the sample lid is closed. Similar to the uptake of acetic acid on these oxide particles, the decrease in the QMS signal is initially the largest and then it gradually drops less. The second time the sample lid is opened, the QMS signal decreases again, but the extent of decrease is not as large as that at the beginning of the experiment when the sample lid was first opened. In the case of SiO_2, the oxide powder was continuously exposed to gas-phase formaldehyde for 200 s. For the heterogeneous uptake of methanol, there is also a change in the QMS signal as a function of time while the oxides are exposed to gas-phase methanol, most notably for uptake on α-Fe_2O_3 and SiO_2.

The observed uptake coefficient for the heterogeneous uptake of acetic acid, formaldehyde, and methanol on the three oxides investigated can be calculated using eq 4. The observed uptake coefficients calculated using eq 4 and using the data shown in Figures 3−5 are presented in Figures 6−8. The values of A_h and A_s used in the calculation are given in each of the figure captions. The data show that the observed uptake coefficient, γ_{obs}, decreases as the oxides are exposed to the reactive gas. The decrease in the uptake coefficient occurs because the surface becomes saturated with adsorbed molecules. Since the uptake coefficient is coverage and, thus, time dependent, it is typical to report an initial uptake coefficient for heterogeneous reaction. In these experiments, the initial uptake coefficient is taken as

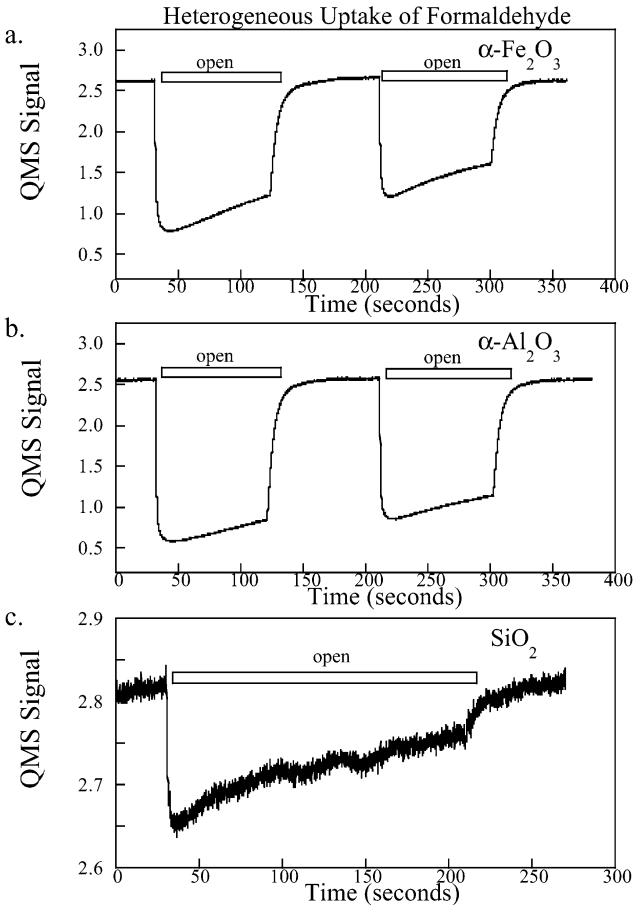

Figure 4. Knudsen cell data (QMS intensity versus time) for the heterogeneous uptake of formaldehyde on 19.6 mg of α-Fe_2O_3, 2.1 mg of α-Al_2O_3, and 2.3 mg of SiO_2. The gas pressure inside the reactor was 6 μTorr measured, and the measured $k_{esc} = 0.20\ s^{-1}$.

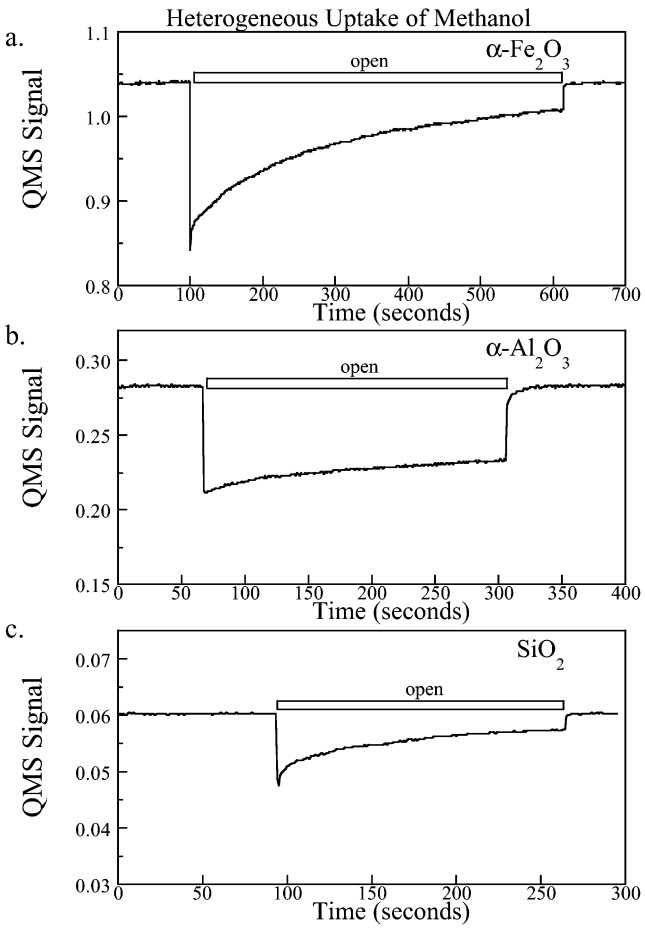

Figure 5. Knudsen cell data (QMS intensity versus time) for the heterogeneous uptake of methanol on 18.8 mg of α-Fe_2O_3, 6.0 mg of α-Al_2O_3, and 6.2 mg of SiO_2. The gas pressure inside the reactor was 2 μTorr measured, and the measured $k_{esc} = 0.56\ s^{-1}$.

the maximum in γ_{obs}, since the response time of the system is convoluted into the measurement.[25]

The data shown in Figures 3−5 and 6−8 are representative Knudsen cell data collected in these experiments. However, there are differences in the data depending on the amount of sample used. One difference observed is that, for a given adsorbate−adsorbent system for large amounts of sample, the uptake of these gases can extend for over several hundreds of seconds whereas, for very small amounts of powder, on the order of a few milligrams, the uptake extends for tens of seconds. The uptake of the gas ceases after the powder is completely saturated. The time it takes to saturate the surface depends on the specific adsorbate−adsorbent system and the total BET area of the powdered sample. Another difference is that the extent of the decreases of the QMS signal also depends on the sample mass. For larger masses the signal decreases more relative to the cases of the smaller masses. This is related to the fact that the observed initial uptake coefficient is mass dependent (vide infra) and underlying layers are contributing to the overall uptake. The mass dependence was investigated in some detail for these VOCs in order to account for the appropriate surface area needed to calculate the initial uptake coefficient.

The heterogeneous uptake of acetic acid, formaldehyde, and methanol was investigated as a function of sample mass and thus the sample surface area. The mass dependence is shown in Figure 9 for acetic acid uptake on α-Fe_2O_3. Three samples of α-Fe_2O_3 of different masses were exposed to acetic acid at a pressure of 6 μTorr for approximately 60 s. For the smallest amount of sample, the QMS intensity signal goes down after the sample lid is open (from $t = 100$ s to $t = 160$ s) and the iron oxide is exposed to acetic acid. It can be seen for the smallest mass that the QMS signal quickly recovers and approaches baseline as the sample becomes saturated with acetic acid. For samples of larger mass and thus a greater amount of total surface area, the initial QMS signal is seen to decrease to a larger extent when the sample lid is in the open position. Not only does the initial signal decrease to a greater extent, but also the signal does not come back to the baseline as quickly, indicating the surface saturates more slowly when there is a greater amount of total surface area. Similar results are obtained for the other adsorbate−adsorbent systems investigated.

These mass dependent data can be used to calculate a true uptake coefficient. The data plotted in Figure 10 show the observed initial uptake coefficient determined for heterogeneous uptake of acetic acid and methanol on α-Fe_2O_3 as a function of sample mass. The data points are shown as solid circles, and a fit to the data using the KML model is shown as the solid line.

The data were fit using a nonlinear least-squares fitting routine, and the results of this fit are given in Figure 10. The experimental parameters used in the KML model are given in the figure caption as well as the fitting parameters, the true initial uptake coefficient, and the tortuosity, τ. For heterogeneous uptake of acetic acid, the true initial uptake coefficient is determined to be 1.9×10^{-3} when the appropriate surface area is taken into account. The data for acetic acid show that the observed uptake coefficient is linear below around 8 mg and that above this mass the plateau region, that is, the mass

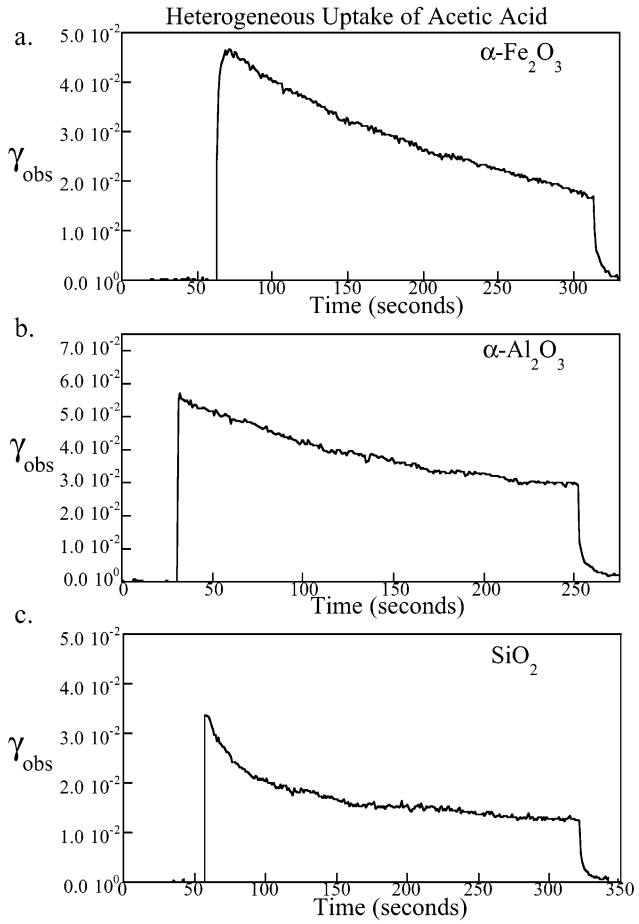

Figure 6. Observed uptake coefficient of acetic acid on α-Fe_2O_3, α-Al_2O_3, and SiO_2 calculated using eq 4 (with $A_s = 5.34$ cm^2 and $A_h = 0.363$ cm^2) and the data shown in Figure 3.

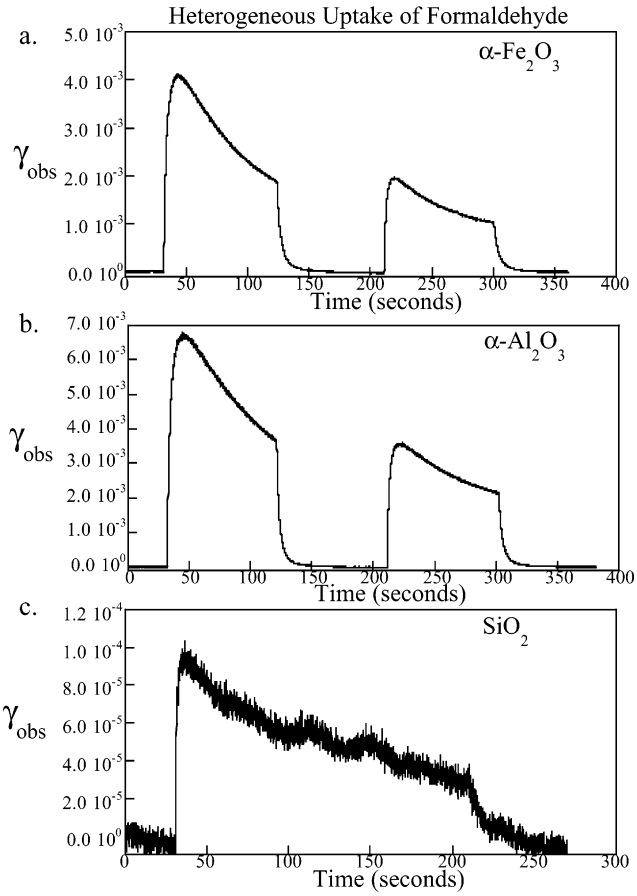

Figure 7. Observed uptake coefficient of formaldehyde on α-Fe_2O_3, α-Al_2O_3, and SiO_2 calculated using eq 4 (with $A_s = 11.96$ cm^2 and $A_h = 0.0445$ cm^2) and the data shown in Figure 4.

independent regime, is seen. For the heterogeneous uptake of methanol, the data are similar in that there is a linear region and a plateau region observed in a plot of γ_{obs} versus mass. However, the linear region is seen to extend out further to 30 mg. The explanation for this difference is that the true uptake coefficient for heterogeneous uptake of methanol on α-Fe_2O_3 is approximately a factor of 10 less than that found for acetic acid. It is expected that diffusion will occur more readily when the true uptake coefficient is smaller; thus, the plateau region will occur at higher masses. The best fit of the data to the KML model is found when the true initial uptake coefficient is 1.9×10^{-4}.

Besides using the KML model to determine the initial uptake coefficient, the linear mass dependent regime can be used as well. This is demonstrated in Figure 10 for methanol uptake on α-Fe_2O_3. The slope of the dotted line shown in Figure 10 is 0.000 93 ($R^2 = 0.95$). Using the value of the slope and eq 7, the true uptake coefficient is calculated to be 1.6×10^{-4}, which is within 15% of that calculated with the KML model. The mass dependence has been measured for heterogeneous uptake of formaldehyde on α-Fe_2O_3 as well as for the heterogeneous uptake of methanol, formaldehyde, and acetic acid on α-Al_2O_3 and SiO_2. Thus, the true uptake coefficients can be determined from either the KML model or the LMD regime for these heterogeneous reactions, and either will give a value that can be used in atmospheric chemistry models. These values are compiled in Table 1.

The kinetic data compiled in Table 1 show that heterogeneous uptake kinetics are greatest for acetic acid on these oxides. In general, organic acids are quite reactive because of the carboxylic functionality present in these compounds. The IR data show that acetic acid irreversibly adsorbs on all three oxides investigated (vide infra). The Knudsen cell data also show that iron oxide and aluminum oxide are in general more active toward the uptake of VOCs, as evidenced by the larger uptake coefficients compared to those for the case of SiO_2. It is expected that SiO_2 would be less reactive than α-Al_2O_3 and α-Fe_2O_3 because the latter oxides have surface sites of greater basic and acidic character compared to SiO_2.[26]

Also shown in Figure 9 is the pressure dependence of the true uptake coefficient for acetic acid on α-Fe_2O_3. The data plotted in Figure 9b are for samples in the linear mass regime, so that the total surface area of the sample was used to calculate the true initial uptake. The value of the true initial uptake is determined to be $(2.0 \pm 0.3) \times 10^{-3}$ in this pressure range. This value is consistent with the value obtained from the data presented in Figure 10a. The data show that the initial uptake coefficient is independent of pressure in this pressure range. The lack of a pressure dependence on the uptake coefficient is consistent with an adsorption process that is first order in gas pressure for the adsorption on α-Fe_2O_3.

In addition to kinetic parameters, the Knudsen cell data can be used to determine surface coverages and whether gas adsorption is reversible or irreversible. Surface coverages were determined by calibrating the mass spectrometer signal to a flow rate (molecules s^{-1}) and then integrating the signal as a function of time to determine the total number of molecules adsorbed on the surface. As described in ref 27, coverage is calculated from the total number of molecules adsorbed on the surface

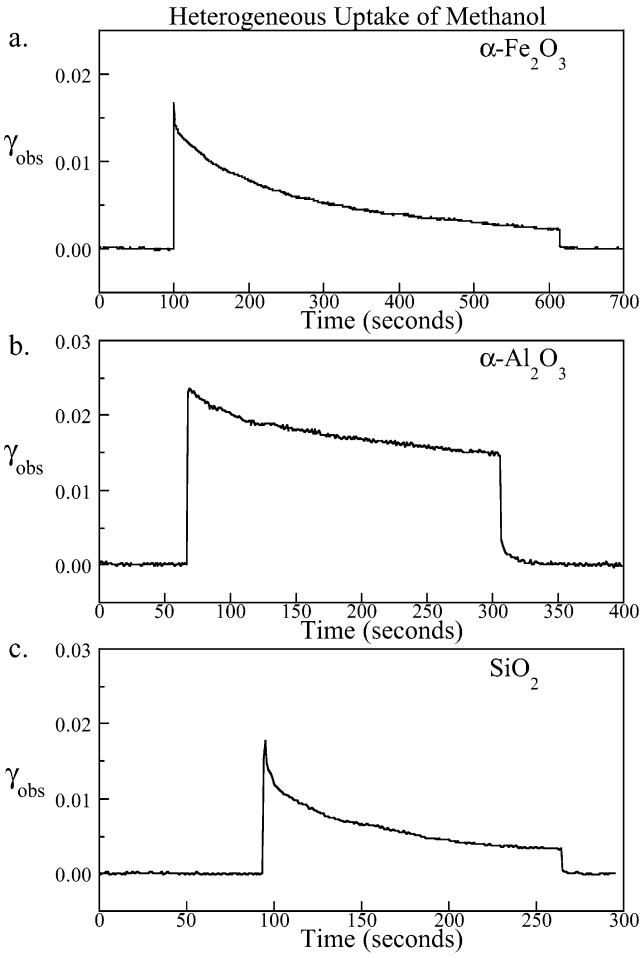

Figure 8. Observed uptake coefficient of methanol on α-Fe_2O_3, α-Al_2O_3, and SiO_2 calculated using eq 4 (with $A_s = 5.34$ cm^2 and $A_h = 0.363$ cm^2) and the data shown in Figure 5.

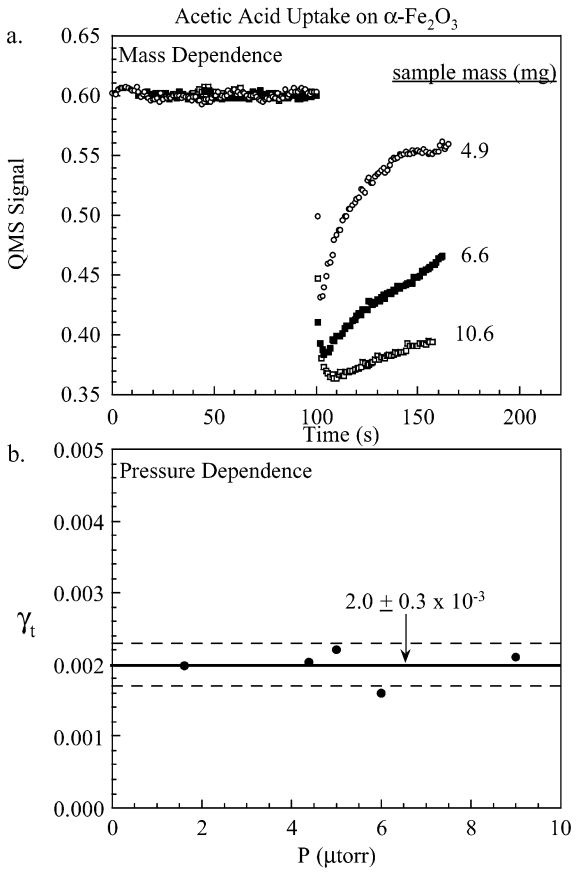

Figure 9. (a) Mass dependence of the uptake of acetic acid on α-Fe_2O_3. Three different masses of α-Fe_2O_3 are shown (open circles, 4.9 mg; filled squares, 6.6 mg; open squares, 10.6 mg). (b) Pressure dependence of the true initial uptake coefficient for acetic acid on α-Fe_2O_3.

divided by total BET surface area. This process must be done for thin samples so that the QMS signal goes back to baseline, indicating surface saturation has occurred. Surface coverages determined in this way are given in Table 2. It can be seen that surface coverages determined for SiO_2 are orders of magnitude lower than those for the two other oxides, indicating less reactivity for SiO_2, as discussed above.

To determine if adsorption of these VOCs is reversible or irreversible, Knudsen cell extraction experiments were done. In these experiments, after the surface had become saturated or equilibrated with the gas phase, the sample lid was lowered to cover the oxide and the leak valve was turned off so that the gas was pumped out by the two-stage pumping system described in the Experimental Section. After the VOC was evacuated from the Knudsen cell reactor system, the sample lid was then raised while the QMS monitored the desorption of the VOC. In the case of acetic acid, methanol, and formaldehyde adsorption on α-Al_2O_3 and α-Fe_2O_3, there was a small amount of desorption back into the gas phase (<1 to 15%). In the case of acetic acid, methanol, and formaldehyde adsorption on SiO_2, there was a significant amount of desorption back into the gas phase (50−100%). To learn more about the nature of the adsorption process, the adsorption of VOCs on oxide surfaces was investigated by transmission FT-IR spectroscopy.

Heterogeneous Uptake of Acetic Acid, Formaldehyde, and Methanol on Oxide Surfaces: FT-IR Measurements. Figures 11−13 show the infrared spectra recorded of acetic acid, methanol, and formaldehyde, respectively, in the spectral range extending from 1000 to 3000 cm^{-1}. The spectra were recorded in the presence of the gas phase at a VOC pressure of around 30 mTorr. Gas-phase absorptions were subtracted from the spectra shown in Figures 11−13 such that only infrared absorptions due to adsorbed species are present. It is found that upon evacuation of the gas phase the spectra did not change very much in terms of the intensities of the peaks or the frequencies of the peaks except in the case for adsorption on SiO_2. For formaldehyde and methanol adsorption on SiO_2, the adsorption process is completely reversible and all infrared absorptions due to adsorbed species disappear upon evacuation of the gas phase. In addition, the frequencies of the infrared absorptions observed for formaldehyde adsorbed on SiO_2 at 1501, 1724, and 2825 cm^{-1} and methanol adsorbed on SiO_2 at 1390, 1452, 1470, 2852, and 3006 cm^{-1} are very close to those in the gas or liquid phase.[28] This suggests that these molecules weakly adsorb on SiO_2. There is also a decrease in intensity of the band at 3748 cm^{-1}, associated with the isolated OH groups, and a concomitant growth of a band at lower frequency near 3420 cm^{-1} (spectral region not shown), suggesting that there is a reversible hydrogen bonding type interaction between these adsorbates and the SiO_2 surface hydroxyl groups.[29−31]

In contrast to the adsorption of formaldehyde and methanol on SiO_2, adsorption is irreversible in part for acetic acid on all three oxides investigated, for methanol on α-Fe_2O_3 and α-Al_2O_3, and for formaldehyde adsorption on α-Fe_2O_3 and α-Al_2O_3. This is to say that, upon evacuation of the gas phase, infrared absorptions associated with surface adsorbed species remain in the spectrum. For the α-Fe_2O_3 and α-Al_2O_3 spectra, the frequencies of many of the infrared absorptions are shifted from

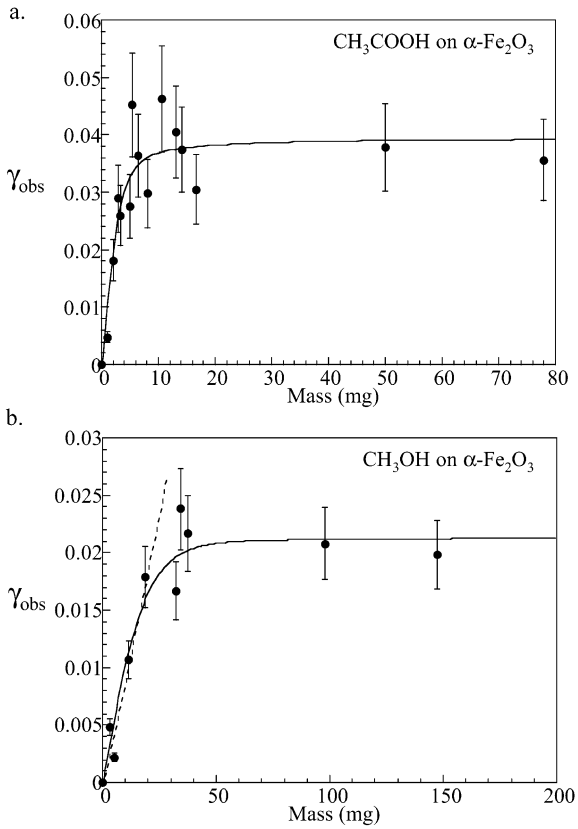

Figure 10. Initial observed uptake coefficient, γ_{obs}, plotted as a function of sample mass (data points represented as filled circles) for heterogeneous uptake of (a) acetic acid on α-Fe_2O_3 and (b) methanol on α-Fe_2O_3. The data are fit to a model which takes into account gas diffusion into the underlying layers, as discussed in the Experimental Section. Experimental parameters include the diameter of the particles, $d = 6.9 \times 10^{-5}$ cm, the bulk density of the iron oxide powder, $\rho_b = 2.1$ mg cm^{-3}, the true density of a continuous slab of iron oxide, ρ_t, of 5.24 mg cm^{-3}, respectively, and the specific BET area of the iron oxide powder, $S_{BET} = 29$ mg cm^{-2}. For methanol uptake on α-Fe_2O_3, nearly all of the data were obtained using the multistage Knudsen cell reactor with $A_h = 5.07$ cm^2. The solid lines are obtained with the fitting parameters for (a) acetic acid uptake on α-Fe_2O_3 [$\gamma_t = 1.9 \times 10^{-3}$ and $\tau = 12$] and for (b) methanol on α-Fe_2O_3 [$\gamma_t = 1.9 \times 10^{-4}$ and $\tau = 3$], and the dotted line shown in part b is the best-fit line determined for the linear regime; see text for further discussion.

TABLE 1: Initial Uptake Coefficients Determined for Acetic Acid, Methanol, and Formaldehyde on Several Oxides[a]

	VOC		
oxide	acetic acid[b]	methanol[c]	formaldehyde[d]
α-Fe_2O_3	$(1.9 \pm 0.3) \times 10^{-3}$	$(1.9 \pm 0.4) \times 10^{-4}$	$(1.1 \pm 0.5) \times 10^{-4}$
α-Al_2O_3	$(2 \pm 1) \times 10^{-3}$	$(1.0 \pm 0.7) \times 10^{-4}$	$(7.7 \pm 0.3) \times 10^{-5}$
SiO_2	$(2.4 \pm 0.4) \times 10^{-4}$	$(4 \pm 2) \times 10^{-6}$	$(2.6 \pm 0.9) \times 10^{-7}$

[a] Error bars were determined by the quality of the fit to the data and experimental reproducibility. [b] The KML model was used to determine the true uptake coefficient for acetic acid on all three oxides. [c] The KML model was used to determine the true uptake coefficient for methanol uptake on α-Fe_2O_3 and α-Al_2O_3. The linear mass dependent (LMD) regime was used to determine the true uptake coefficient for methanol uptake on SiO_2. [d] The linear mass dependent (LMD) regime was used to determine the true uptake coefficient for formaldehyde uptake on all three oxides.

those in the gas or liquid phase,[28] as is the case for irreversible adsorption. In the case of acetic acid and methanol adsorption, many of the spectral features in the α-Fe_2O_3 and α-Al_2O_3 spectra are consistent with the presence of acetate (CH_3COO^-)[32-37] and methoxide (CH_3CO^-),[38-42] respectively, on the oxide surfaces.

TABLE 2: Surface Coverages[a] Determined for Acetic Acid, Methanol, and Formaldehyde on Several Oxides

	VOC		
oxide	acetic acid (6 μTorr)	methanol (2 μTorr)	formaldehyde (6 μTorr)
α-Fe_2O_3	$(5 \pm 3) \times 10^{13}$	$(2 \pm 1) \times 10^{13}$	$(2 \pm 1) \times 10^{13}$
α-Al_2O_3	$(8 \pm 4) \times 10^{13}$	$(2 \pm 1) \times 10^{13}$	$(2 \pm 1) \times 10^{13}$
SiO_2	$(7 \pm 3) \times 10^{11}$	$(8 \pm 4) \times 10^{11}$	$(1.1 \pm 0.5) \times 10^{11}$

[a] Surface coverages, in units of molecules cm^{-2}, measured at the pressures noted in parentheses below each VOC. Errors in the measurement are determined from multiple experiments.

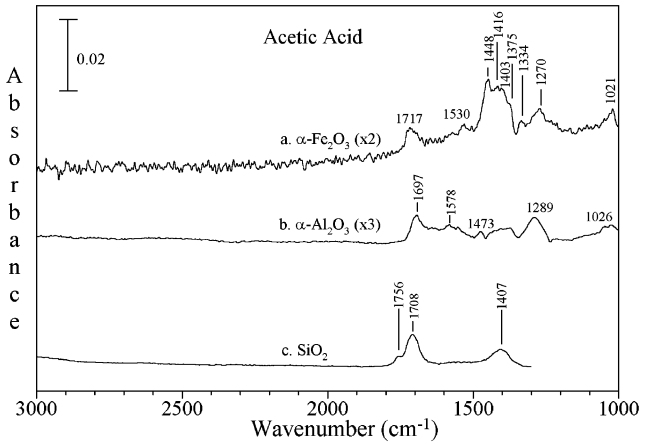

Figure 11. Transmission FT-IR spectra of acetic acid adsorbed on α-Fe_2O_3, α-Al_2O_3, and SiO_2 in the presence of gas-phase acetic acid at a pressure of approximately 30 mTorr. Gas-phase absorptions have been subtracted from the above spectra. SiO_2 infrared data are cut off at 1300 cm^{-1}, because of intense lattice absorptions.

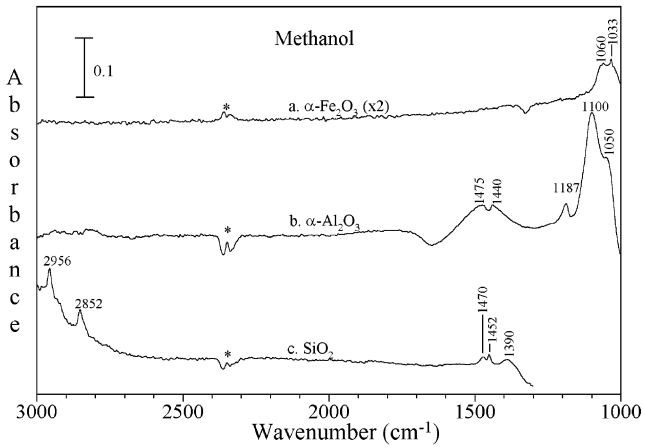

Figure 12. Transmission FT-IR spectra of methanol adsorbed on α-Fe_2O_3, α-Al_2O_3, and SiO_2 in the presence of gas-phase methanol at a pressure of approximately 30 mTorr. Gas-phase absorptions have been subtracted from the above spectra. SiO_2 infrared data are cut off at 1300 cm^{-1}, because of intense lattice absorptions. Features indicated with an asterisk are due to the dry-air purge and poor cancellation of gas-phase CO_2 absorptions.

For formaldehyde adsorption on α-Fe_2O_3 and α-Al_2O_3, there may be several irreversibly adsorbed species on the surface, such as formate and methoxide.[43,44] The infrared data are in agreement with the Knudsen cell experiments which show that adsorption for most molecules is nearly completely irreversible for α-Fe_2O_3 and α-Al_2O_3.

Atmospheric Implications and the Effect of Relative Humidity on Heterogeneous Uptake Kinetics of VOCs on Oxides. Little is known about the heterogeneous chemistry of

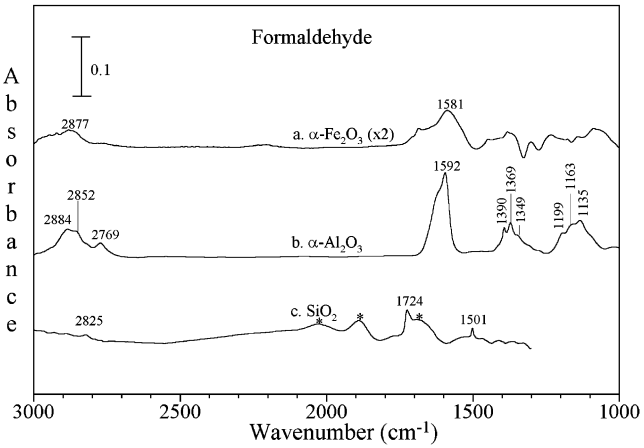

Figure 13. Transmission FT-IR spectra of formaldehyde adsorbed on α-Fe_2O_3, α-Al_2O_3, and SiO_2 in the presence of gas-phase formaldehyde at a pressure of approximately 30 mTorr. Gas-phase absorptions have been subtracted from the above spectra. SiO_2 infrared data are cut off at 1300 cm^{-1}, because of intense lattice absorptions. Features indicated with an asterisk are due to SiO_2 lattice absorptions that did not subtract out well in the difference spectrum.

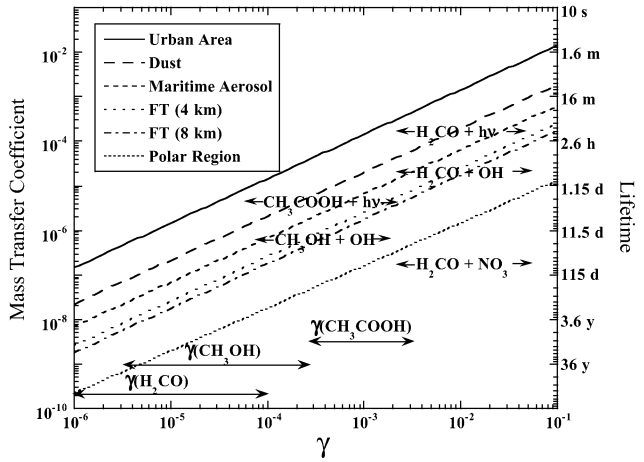

Figure 14. Calculated mass transfer coefficients as a function of the heterogeneous uptake γ, as described in the text and ref 14. Gas-phase photolysis rates and other loss rates due to reaction with OH and NO_3 are shown for comparison. This diagram shows that under certain conditions loss rates of formaldehyde, acetic acid, and methanol through heterogeneous uptake are comparable to those of other mechanisms.

organics. However, it is clear that organics play a critical role in the troposphere and the photochemical oxidant cycle. If heterogeneous chemistry is to be important in these systems, then the reactions must be fast enough to be competitive with known gas-phase chemical and photochemical reactions in order to have an appreciable effect on the chemical balance of the troposphere. Although the complexity of mineral dust aerosol is much greater than that of the oxide particles investigated here, it is proposed that these particles can be used as model systems and represent a first step toward understanding the chemistry on mineral dust aerosol.

In a previous paper,[16] we expressed the rates of heterogeneous reactions in terms of a pseudo-first-order mass transfer rate constant. From this rate constant, the lifetime of gas-phase molecules due to heterogeneous uptake can be calculated. The data for these calculations are shown in the double-*y* plot shown in Figure 14, where the pseudo-first-order mass transfer rate constant and the lifetime are calculated as a function of γ. Since the total surface area available for reaction plays a role in heterogeneous chemistry, the pseudo-first-order mass transfer rate constant is calculated as a function of different aerosol size distributions and particle densities. These distributions are labeled as urban area, dust, maritime aerosol, free troposphere (FT), at 4 and 8 km from the Earth's surface, and polar region.[45−47] More of the details of these distributions are given in Table 3 and described in ref 16.

TABLE 3: log−Normal Distributions Used To Calculate Heterogeneous Loss Rates[a,b]

	no. mode[c]	n_i[d]	R_i[e]	log(σ_i)[f]
polar	I	21.7	0.0689	0.245
	II	0.186	0.375	0.300
	III	0.000304	4.29	0.291
troposphere	I	129	0.0036	0.645
ind(background)[g]	II	59.7	0.127	0.253
	III	63.5	0.259	0.425
maritime	I	133	0.0039	0.657
	II	66.6	0.133	0.210
	III	3.06	0.29	0.396
urban	I	99300	0.00651	0.245
	II	1110	0.00714	0.666
	III	36400	0.0248	0.337
dust	I	7.98	0.88	0.23

[a] See refs 14 and 27−29. [b] Other conditions: diffusivity, 0.148 cm^2 s^{-1}; density, 2.0 g/cm^3; mean free path, 0.07 μm (in the boundary layer), 0.10 μm (at 4 km), 0.16 μm (at 8 km). [c] No. mode is the modal distribution used. [d] n_i is the cumulative particle number distribution in cm^{-3}. [e] R_i is the mean particle radius in μm. [f] log σ_I is a measure of particle polydispersity. [g] The major difference between the background in the boundary layer and at 4 km and 8 km is the mean free path.

The importance of heterogeneous reactions is determined by whether they are competitive with other known sinks, that is, other removal and loss processes.[48] This is demonstrated here for some known sinks of formaldehyde, acetic acid, and methanol. The most important sinks for formaldehyde are through photolysis and reactions with OH and NO_3. The kinetics, in terms of atmospheric lifetimes of formaldehyde associated with these three processes, are superimposed on the plot in Figure 14. For a heterogeneous uptake of 10^{-6}, it is seen that the heterogeneous reaction is not competitive with the other loss mechanisms under any conditions. At a heterogeneous uptake coefficient in the 10^{-4} range, the heterogeneous pathway becomes competitive with the NO_3 reaction for all aerosol distributions excluding that for the polar region. For the aerosol distribution labeled dust, it is seen that the heterogeneous pathway is much faster than the NO_3 reaction and begins to compete with the OH reaction for $\gamma > 10^{-4}$. The values of γ measured here would indicate that the heterogeneous uptake on mineral dust containing iron and aluminum oxide could contribute as a removal mechanism for formaldehyde. Further modeling analysis of the heterogeneous removal of formaldehyde would need to consider how surface deactivation, as indicated by the laboratory data, would affect these conclusions.

One gas-phase sink for acetic acid is through photolysis. The atmospheric lifetime of acetic acid from loss due to photolysis is 1.3 days. Thus, the heterogeneous uptake of acetic acid calculated for the dust and urban area distributions is competitive with the photolysis loss mechanism for acetic acid with initial uptake coefficients on the order of 10^{-3} to 10^{-4}, close to the value measured here.

In the case of methanol, one important sink is through reaction with hydroxyl radical. This reaction leads to the production of the peroxide radical and formaldehyde, which is another source of radicals in the atmosphere. Thus, irreversible loss of methanol through heterogeneous uptake could lead to a reduction of radical species in the troposphere. The lower uptake coefficients measured for the heterogeneous uptake of methanol are com-

petitive with the hydroxyl radical reaction when the urban area, dust, and maritime aerosol distributions are used in the calculation.

It is important to note that these experiments have all been done under dry conditions whereas the appropriate relative humidity (RH) of the troposphere is between 20 and 90%. Thus, water vapor pressures at 295 K would be expected to be somewhere between 2 and 20 Torr. It is estimated from FT-IR spectroscopy that there are approximately two layers of water on the particle surface at a relative humidity of 50%.[49] From information in the literature for heterogeneous reaction kinetics of acetic acid, formaldehyde, and methanol with water droplets and for effects of RH on VOC adsorption on oxides, we can extrapolate and discuss the potential effects of RH and water adsorption on the heterogeneous reaction kinetics of the VOCs investigated here.

For inorganic acids, such as nitric acid, surface adsorbed water enhances the uptake of nitric acid on oxide surfaces by at least 1 order of magnitude relative to dry conditions.[49] Therefore, it is anticipated that for organic acids, such as acetic acid, the heterogeneous uptake coefficient should depend on water vapor pressure and surface adsorbed water. If a similar order of magnitude enhancement occurred for acetic acid uptake on the oxides investigated here, the value of the initial uptake coefficient would approach 0.01. This value is approximately a factor of 2 lower than the value for heterogeneous uptake of acetic acid by water droplets at 295 K.[50,51]

For methanol and formaldehyde, the prediction is less clear. The mass accommodation coefficient has been measured for methanol and formaldehyde on water droplets.[50−52] The values of the uptake coefficient are on the order of 10^{-2}, larger than the heterogeneous uptake coefficients measured here for these compounds on oxide surfaces. If wetted oxide particles behaved like a water droplet, it would be expected that the heterogeneous uptake coefficient would increase as a function of relative humidity. The mechanism for uptake could then change and would involve the dissolution of the organic in the thin water film, estimated at 50% RH to be around two layers. Studies by Goss and co-workers[12,53] show that under certain conditions of relative humidity there is a competition between water and organic molecules for adsorption sites on the oxide surface. Thus, there is the possibility that the heterogeneous reaction probability could actually decrease for these molecules under some conditions.

Although further laboratory studies on the effect of RH on the heterogeneous uptake of VOCs along with additional modeling analysis are needed in order to fully understand the role of heterogeneous chemistry of VOCs on mineral dust and other atmospheric particles, it is interesting to note that there is some potential for these reactions to be competitive with known gas-phase chemical and photochemical reactions. Future analysis would need to include the coverage dependent uptake coefficient, the fact that mineral dust surfaces may become saturated with time in the atmosphere as well, and the relative humidity dependence on these processes. For reversible adsorption such as that found for methanol and formaldehyde adsorption on SiO_2, adsorption isotherms will be important for determining surface coverages as a function of pressure, as has been measured for organics on ice surfaces.[53−56] These issues are currently under investigation.

Acknowledgment. This research was supported by the Biological and Environmental Research Program (BER), U.S. Department of Energy, Grant No. DE-FG02-98ER62580. The authors gratefully acknowledge Professor Gregory Carmichael for his assistance in the modeling aspects of this study.

References and Notes

(1) Lurmann, F. W.; Loyd, A. C.; Atkinson, R. A. *J. Geophys. Res., [Atmos.]* **1986**, *91*, 10905.
(2) Ryerson, T. B.; Trainer, M.; Holloway, J. S.; Parrish, D. D.; Huey, L. G.; Sueper, D. T.; Frost, G. J.; Donnelly, S. G.; Schauffler, S.; Atlas, E. L.; Kuster, W. C.; Goldan, P. D.; Hübler, G.; Meagher, J. F.; Fehsenfeld, F. C. *Science* **2001**, *292*, 719.
(3) Seinfeld, J. H.; Pandis, S. N. *Atmospheric Chemistry and Physics: From Air Pollution to Climate Change*; John Wiley and Sons: New York, 1998.
(4) Finlayson-Pitts, B. J.; Pitts, J. N. *Chemistry of the Upper and Lower Atmosphere: Theory, Experiments and Applications*; Academic Press: San Diego, CA, 2000.
(5) Singh, H.; Chen, Y.; Staudt, A.; Jacob, D.; Blake, D.; Heider, B.; Snow, J. *Nature* **2001**, *410*, 1078.
(6) Atkinson, R. *Atmos. Environ.* **2000**, *34*, 2063.
(7) Singh, H.; Chen, Y.; Tabazadeh, A.; Fukui, Y.; Bey, I.; Yantosca, R.; Jacob, D.; Arnold, F.; Wohlfrom, K.; Atlas, E.; Flocke, F.; Blake, D.; Blake, N.; Heikes, B.; Snow, J.; Ralbot, R.; Gregory, G.; Sachse, G.; Vay, S.; Kondo, Y. *J. Geophys. Res., [Atmos.]* **2000**, *105*, 3795.
(8) Khare, P.; Kumar, K.; Kumari, K. M.; Srivastava, S. S. *Rev. Geophys.* **1999**, *37*, 227.
(9) Chebbi, A.; Carlier, P. *Atmos. Environ.* **1996**, *30*, 4233.
(10) Lee, S.-H.; Murphy, D. M.; Thomson, D. S.; Middlebrook, A. M. *J. Geophys. Res., [Atmos.]* **2002**, *107*, DOI: 10.1029/2000JD000011.
(11) Russell, L. M.; Maria, S. F.; Myeni, S. C. B. *Geophys. Res. Lett.* **2002**, *29*, DOI: 10.1029/2002GL014874.
(12) Goss, K. U.; Schwarzenbach, R. P. *Environ. Sci. Technol.* **1999**, *33*, 4073.
(13) Golden, D. M.; Spokes, G. N.; Benson, S. W. *Angew. Chem., Int. Ed. Engl.* **1973**, *12*, 534.
(14) Caloz, F.; Fenter, F. F.; Tabor, K. D.; Rossi, M. J. *Rev. Sci. Instrum.* **1997**, *68*, 3172.
(15) Golden, D. M.; Manion, J. A. *Advances in Chemical Kinetics and Dynamics*, Vol. 1; JAI Press: 1992; pp 187−276.
(16) Li, P.; Perreau, K. A.; Covington, E.; Carmichael, G. C.; Grassian, V. H. *J. Geophys. Res., [Atmos.]* **2001**, *106*, 5517−5529. For the formaldehyde experiments a larger single-stage Knudsen cell reactor was used; the reactor is described in ref 14.
(17) Miller, T. M.; Grassian, V. H. *Geophys. Res. Lett.* **1998**, *25*, 3835.
(18) Amman, M.; Poschl, U.; Rudich, Y. *Phys. Chem. Chem. Phys.*, in press.
(19) Underwood, G. M.; Li, P.; Usher, C.; Grassian, V. H. *J. Phys. Chem. A* **2000**, *104*, 819.
(20) Aris, R. *The Mathematical Theory of Diffusion and Resaction in Permeable Catalysts*, Vol. I; Clarendon Press: Oxford, U.K., 1975.
(21) Keyser, L. F.; Moore, S. B.; Leu, M.-T. *J. Phys. Chem.* **1991**, *95*, 5496.
(22) Keyser, L. F.; Leu, M.-T.; Moore, S. B. *J. Phys. Chem.* **1993**, *97*, 2800.
(23) Fenter, F. F.; Caloz, F.; Rossi, M. J. *J. Phys. Chem.* **1996**, *100*, 1008.
(24) Grassian, V. H. *J. Phys. Chem. A* **2002**, *106*, 860.
(25) Li, P.; Al-Abadleh, H. A.; Grassian, V. H. *J. Phys. Chem. A* **2002**, *106*, 1210.
(26) Morrison, S. R. *The Chemical Physics of Surfaces*; Plenum Press: New York and London, 1990.
(27) Underwood, G. M.; Li, P.; Al-Abadleh, H.; Grassian, V. H. *J. Phys. Chem. A* **2001**, *105*, 6609.
(28) NIST Reference Data (http://webbook.nist.gov/chemistry/).
(29) Hair, M. L. *Infrared Spectroscopy in Surface Chemistry*; Marcel Dekker: New York, 1967.
(30) Little, L. H. *Infrared Spectra of Adsorbed Species*; Academic: London, 1966.
(31) Pimentel, G. C.; McClellan, A. L. *The Hydrogen Bond*; Freeman: San Francisco, CA, 1960.
(32) Finocchio, E.; Willey, R. J.; Busca, G.; Lorenzelli, V. *J. Chem. Soc., Faraday Trans.* **1997**, *93*, 175.
(33) Tanaka, H.; Watanabe, T.; Chikazawa, M. *J. Chem. Soc., Faraday Trans.* **1997**, *93*, 4377.
(34) Quiles, F.; Burneau, A. *Vib. Spectrosc.* **1998**, *16*, 105.
(35) Shimizu, K.-I.; Kawabata, H.; Satsuma, A.; Hattori, T. *J. Phys. Chem. B* **1999**, *103*, 5240.
(36) Ferri, D.; Burgi, T.; Baiker, A. *J. Chem. Soc., Perkins. Trans 2*: *Phys. Org. Chem.* **1999**, *7*, 1305.
(37) Kubicki, J. D.; Schroeter, L. M.; Itoh, M. J.; Nguyen, B. N.; Apitz, S. E. *Geochim. Cosmochim. Acta* **1999**, *63*, 2709.
(38) Wadayama, T.; Suzuki, O.; Takeuchi, K.; Seki, H.; Tanabe, T.; Suzuki, Y.; Hatta, A. *Appl. Phys. A: Mater. Sci. Process.* **1999**, *69*, 77.

(39) Beebe, T. P., Jr.; Crowell, J. E.; Yates, J. T., Jr. *J. Chem. Phys.* **1990**, *92*, 5119.
(40) Beebe, T. P., Jr.; Crowell, J. E.; Yates, J. T., Jr. *J. Phys. Chem.* **1988**, *92*, 1296.
(41) Busca, G.; Rossi, P. F.; Lorenzelli, V.; Benaissa, M.; Travert, J.; Lavalley, J. C. *J. Phys. Chem.* **1985**, *89*, 5433.
(42) Clarke, D. B.; Lee, D.-K.; Sandoval, M. J.; Bell, A. T. *J. Catal.* **1994**, *150*, 81.
(43) Busca, G.; Lorenzelli, V. *J. Catal.* **1980**, *66*, 155.
(44) Busca, G.; Lamotte, J.; Lavalley, J. C.; Lorenzelli, V. *J. Am. Chem. Soc.* **1987**, *109*, 5197.
(45) Jaenicke, R.; Hanusch, T. *Aerosol Sci. Technol.* **1993**, *18*, 309.
(46) Zhang, Y. Ph.D. Dissertation, Department of Chemical and Biochemical Engineering, The University of Iowa, 1994.
(47) Zhang, Y.; Sunwoo, Y.; Carmichael, G.; Kotamarthi, V. *J. Appl. Meteorol.* **1994**, *33*, 813.
(48) Chemical Kinetics and Photochemical Data for Use in Stratospheric Modeling, JPL Publication 00-3, 2000 (Can be found at http://jpldataeval-.jpl.nasa.gov).
(49) Goodman, A. L.; Bernard, E. B.; Grassian, V. H. *J. Phys. Chem. A* **2001**, *105*, 6443−6457.
(50) Jayne, J. T.; Duan, S. X.; Davidovits, P.; Worsnop, D. R.; Zahniser, M. S.; Kolb, C. E. *J. Phys. Chem.* **1991**, *95*, 6329.
(51) Davidovits, P.; Jayne, J. T.; Duan, S. X.; Worsnop, D. R.; Zahniser, M. S.; Kolb, C. E. *J. Phys. Chem.* **1991**, *95*, 6337.
(52) Jayne, J. T.; Duan, S. X.; Davidovits, P.; Worsnop, D. R.; Zahniser, M. S.; Kolb, C. E. *J. Phys. Chem.* **1992**, *96*, 5452.
(53) Goss, K. U. *Environ. Sci. Technol.* **1992**, *26*, 2287.
(54) Hudson, P. K.; Zondlo, M. A.; Tolbert, M. A. *J. Phys. Chem. A* **2002**, *106*, 2882.
(55) Sokolov, O.; Abbatt, J. P. D. *J. Phys. Chem. A* **2002**, *106*, 775.
(56) Winkler, A. K.; Holmes, N. S.; Crowley, J. N. *Phys. Chem. Chem. Phys.* **2002**, *4*, 5270.